

Inverse problems of generalized projection operators

Mikko Kaasalainen¹ and Lars Lamberg

Department of Mathematics and Statistics, University of Helsinki, PO Box 68, FIN-00014, Finland

E-mail: mikko.kaasalainen@helsinki.fi

Received 28 September 2005, in final form 19 February 2006

Published 11 April 2006

Online at stacks.iop.org/IP/22/749

Abstract

We introduce the concept of generalized projection operators, i.e., projection integrals over a body in \mathbb{R}^3 that generalize the usual result of projected area in a given direction by taking into account shadowing and scattering effects as well as additional convolution functions in the integral. Such operators arise naturally in connection with various observation instruments and data types. We review and discuss some properties of these operators and the related inverse problems, particularly in the cases pertaining to photometric and radar data. We also prove an ambiguity theorem for a special observing geometry common in astrophysics, and uniqueness theorems for radar inverse problems of a spherical target. These theorems are obtained by employing the intrinsic rotational properties of the observing geometries and function representations. We then present examples of the mathematical modelling of the shape and rotation state of a body by simultaneously using complementary data sources corresponding to different generalized projection operators. We show that generalized projection operators unify a number of mathematical considerations and physical observation types under the same concept.

1. Introduction

Projections or silhouettes are a natural and abundant source of information in, e.g., human and computer vision, cartography and astrophysics. In the last one, projections on the plane-of-sky constitute a typical data mode due to the long distances between the target and the observer. Often the distance is for all practical purposes infinite, i.e., the ratio of the size of the object and the distance approaches zero with all instruments. In such cases the projection is not disc-resolved, and the only observable quantities are related to the projection area, leading to interesting inverse problems.

In mathematics, certain problems in this field are sometimes called geometric tomography (often with the inclusion of volumes of sections in addition to those of projections), although

¹ Rolf Nevanlinna Institute; also Sodankylä Geophysical Observatory, 99600 Sodankylä, Finland.

the problems are not tomography in the usual sense, i.e., we do not obtain information on the interior of the target as in the case of Radon transforms and other tomographic methods. However, often the information obtained is not about the exact areas of the projections (with which geometric tomography is concerned), but certain generalizations of the concept. In the following, we use the term ‘generalized projection operator’ to denote the operator \mathcal{P} that yields these generalized projection areas from an object in \mathbb{R}^3 . The operator is represented by a projection integral, and the generalizations are due to various physical reasons:

- (i) shadowing effects, i.e., the object is illuminated and viewed from different directions ($S^2 \times S^2$ instead of S^2);
- (ii) light-scattering effects, i.e., additional weight functions in the projection integral;
- (iii) additional convolution functions in the integral introducing various dimensions of data space (e.g., in astrophysics we have $S^2 \times S^2 \times S^1$ for interferometry, and $S^2 \times \mathbb{R}^2$ for monostatic range-Doppler radar).

Inverse problems of generalized projection operators are of mathematical interest since while the problem of shape reconstruction from the volumes of simple projections is nonunique, the generalized projections carry much more information and yield strong uniqueness properties as we will show in this paper. This makes them highly useful for the mathematical modelling of observations with various instruments in physical sciences. Generalized projection operators thus unify a number of mathematical considerations and physical observation types under the same concept.

The paper is organized as follows: in section 2 we define various types of generalized projection operators (corresponding to data types such as photometry, interferometry and radar experiments), and in section 3 we review essential developments and related uniqueness and other theorems in the photometric case as well as prove a mild ambiguity theorem affecting many astrophysical observations. In section 4 we prove uniqueness theorems for range- and Doppler-resolution radar observations and discuss their information contents. In section 5 we discuss the strong usefulness of combining several data modes in what we call multidata inversion, and as case studies present two astrophysical examples related to the combination of radar or interferometric data with photometry. In section 6 we sum up and discuss various details of the problems and data types presented in this paper. The three appendices contain mathematical information employed in the analysis in the main text.

2. Generalized projection operators

Let $\omega \in S^2$ be the viewing direction (unit vector in \mathbb{R}^3) of the surface of the object \mathcal{B} in \mathbb{R}^3 (\mathcal{B} is arbitrary: it can be nonconvex, topologically different from S^2 , non-starlike, disconnected bodies, etc). The centroid of \mathcal{B} is usually placed at the origin for practical purposes, but this choice can also be left arbitrary. Here we assume the object to be at infinity, i.e., so far away that the unit vector from a surface point to the viewer is the same for all points of \mathcal{B} (and its direction is ω). This assumption can be relaxed in a completely straightforward manner, so we do not discuss such generalizations here.

2.1. $\mathcal{P}(\omega)$

The generalized projection area L is obtained by the projection operator \mathcal{P} operating on the object: $L(\omega) = \mathcal{P}(\omega)\mathcal{B}$. In the case of simple projections (also called geometric scattering), the kernel P is

$$P = \mu(\omega) := \langle \omega, \eta \rangle, \quad (1)$$

where η is the outward unit normal of a surface patch $d\sigma$, and the integration region $A^+(\omega)$ is over the parts of \mathcal{B} for which $\mu \geq 0$ and the line from the surface point in the direction of ω intersects no parts of \mathcal{B} . Thus

$$L(\omega) = \mathcal{P}(\omega)\mathcal{B} = \iint_{A^+(\omega)} P(\omega) d\sigma = \iint_{A^+(\omega)} \mu(\omega) d\sigma. \quad (2)$$

In the more general case, P is given by

$$P(\omega) = S(\mu)\rho, \quad (3)$$

where the expression $S(\mu)$ represents a physical scattering model, and ρ is the intrinsic brightness (reflectivity function) of the surface; often one sets $\rho \equiv 1$. Typically, S is a linear combination of powers of μ .

2.2. $\mathcal{P}(\omega_0, \omega)$

The general photometric projection operator uses two directions ω_0, ω (illumination and viewing), so now we have

$$L(\omega_0, \omega) = \iint_{A^+(\omega_0, \omega)} P(\omega_0, \omega) d\sigma, \quad (4)$$

where $A^+(\omega_0, \omega) := A^+(\omega_0) \cap A^+(\omega)$,

$$P(\omega_0, \omega) = S(\mu_0, \mu, \alpha)\rho, \quad (5)$$

$\alpha := \arccos(\langle \omega_0, \omega \rangle)$, $\mu_0(\omega_0) := \langle \omega_0, \eta \rangle$, and a typical form for S is, e.g., a linear combination of the Lommel–Seeliger and Lambert scattering models, multiplied by some function of the illumination phase α :

$$S = f(\alpha)\mu\mu_0 \left(\frac{1}{\mu + \mu_0} + c \right) \quad (6)$$

(c is a constant or a location-dependent function). This and other scattering models (including more complex forms) are discussed in [8, 10]. The properties of this operator are reviewed and discussed in section 3.

2.3. $\mathcal{P}(\omega, \mathcal{D}, d)$

Radar experiments introduce two new data dimensions: range (or line-of-sight depth, proportional to the delay of the signal) d and Doppler frequency if the object is rotating. The latter is directly proportional to the line-of-sight (Doppler) velocity \mathcal{D} of a surface point, so we can choose \mathcal{D} to be our observable here. Here we use a coordinate system in which the z -axis coincides with the rotation axis of the target. We consider the monostatic S^2 -case in which one antenna both transmits and receives ($\omega_0 = \omega$).

The delay-Doppler radar projection operator $\mathcal{P}(\omega, \mathcal{D}, d)$ has the same kernel as $\mathcal{P}(\omega)$, but the integration region is the subset of those points $\mathbf{x} = (x, y, z) \in \mathcal{B}$ of A^+ for which (when d is chosen to increase towards the observer and positive \mathcal{D} corresponds to approaching motion)

$$d = (x \cos \varphi + y \sin \varphi) \sin \theta + z \cos \theta, \quad \mathcal{D} = w \sin \theta (x \sin \varphi - y \cos \varphi), \quad (7)$$

where w is a positive constant (2π /rotation period) and

$$\omega = \omega(\theta, \varphi) := (\sin \theta \cos \varphi, \sin \theta \sin \varphi, \cos \theta), \quad 0 \leq \theta \leq \pi, 0 \leq \varphi \leq 2\pi, \quad (8)$$

θ and φ being, respectively, the usual polar and azimuthal spherical coordinates. The projection of a curve of constant \mathcal{D} in the direction of ω on a plane to which ω is normal is thus parallel

to the corresponding projection of the rotation axis, and θ is the angle between the spin vector and the line of sight. This definition yields L as a density function over \mathcal{D} and d , so in practice the observable $L(\omega, \mathcal{D}, d)$ at discrete (binned) intervals of d and \mathcal{D} is given by keeping the usual A^+ as the integration region, but with the kernel

$$P(\omega, \mathcal{D}, d) = T_{\mathcal{D}}(\mathcal{D} - \mathcal{D}')T_d(d - d')S(\mu_0, \mu)\rho, \quad (9)$$

where $T_{\mathcal{D}}, T_d$ are peaked locally sampling functions (equivalent to the above if $T(x - x') = \delta(x - x')$). Here primed variables in the kernel are integration variables corresponding to the surface patches $d\sigma$. The properties of this operator are discussed in section 4, where we will also use a practical renormalized form \hat{D} for the Doppler variable:

$$\hat{D} := \frac{\mathcal{D}}{w \sin \theta}, \quad -1 \leq \hat{D} \leq 1. \quad (10)$$

2.4. $\mathcal{P}(\omega_0, \omega, s)$

The interferometric projection operator projects \mathcal{B} on S^2 (plane-of-sky) and has a convolution kernel for $s \in S^1$ along a great circle on that S^2 :

$$P(\omega_0, \omega, s) = T(s - s')S(\mu_0, \mu, \alpha)\rho, \quad (11)$$

where $s' \in S^1$ is the point on the great circle closest to the projection of a point of \mathcal{B} on S^2 . The convolving function is caused by the optical interference pattern of the instrument, and is typically close to the following theoretical point-source point-spread function [5]:

$$T(s) \approx -\frac{\sin^2 z}{z}, \quad z := \frac{2\pi R}{\lambda}s, \quad (12)$$

where R is the aperture of the instrument and λ is the wavelength. We discuss this operator in section 5.

With interferometric data, we start to move from infinity to finite distances, i.e., the projection of \mathcal{B} on S^2 has a nonvanishing size. The next step is the possibility of forming actual disc-resolved though strongly convolved images through, e.g., adaptive optics [19]. These correspond to the operator $\mathcal{P}(\omega_0, \omega, \Omega)$, with $\Omega \in S^2$, that reads like the radar one, but with Ω instead of (d, \mathcal{D}) . In practice

$$P(\omega_0, \omega, \Omega) = T_{\Omega}(\Omega - \Omega')S(\mu_0, \mu, \alpha)\rho, \quad (13)$$

where T_{Ω} ranges from almost constant (the object is almost at infinity) to $\delta^{(2)}$ (completely disc-resolved image).

There is thus a continuum of projection operations from infinite to finite distances, or from remote sensing to cartography. Radar projection is unique in its ability to sample subsets of A^+ at infinity.

3. Photometric operator

The nonuniqueness of shape reconstruction in pure geometric tomography is well known, and demonstrated in, e.g., the Blaschke bullet (the two-dimensional analogue of which is the Reuleaux triangle). This property was shown by Russell [26]; related discussion and analysis has a long timeline from Blaschke in the 1910s and Aleksandrow in the 1930s to present (see, e.g., [3, 4] and references therein). If we consider generalized projection operators, the nonuniqueness vanishes already with S^2 -data for certain scattering functions, as discussed in [7, 8]. However, in many realistic situations the scattering function is close to geometric in

the S^2 -case, so the nonuniqueness condition can be removed only by extending the data to $S^2 \times S^2$.

The uniqueness proof of the inversion of the general photometric projection operator (with convex bodies and data in $S^2 \times S^2$) was given by Kaasalainen [7, 8], who also showed that certain functional forms of the scattering function S allow unique solutions for its subfunctions (including location dependence) in addition to shape reconstruction. Further properties of this operator were discussed and proved by Lamberg [16], who especially showed that the inverse of this operator is continuous in the *weak**-topology, and that the inverse problem would be uniquely solvable and at the same time completely independent of the scattering function S if we could use certain limiting values at $\alpha \rightarrow \pi$ as our data set. We briefly state the relevant theorems here for completeness (for proofs see [7, 8, 16]).

Let the surface of a convex compact body be given by the Gaussian image $\mathbf{x}(\eta)$, $\eta = \vartheta(\vartheta, \psi)$, $0 \leq \vartheta \leq \pi$, $0 \leq \psi \leq 2\pi$. The surface patch $d\sigma(\eta)$ is given by

$$G(\eta) \sin \vartheta \, d\vartheta \, d\psi, \quad (14)$$

where the curvature function $G \geq 0$ is

$$G(\vartheta, \psi) = \frac{|\mathbf{J}(\vartheta, \psi)|}{\sin \vartheta}, \quad (15)$$

and \mathbf{J} is the Jacobian

$$\mathbf{J}(\vartheta, \psi) = \frac{\partial \mathbf{x}}{\partial \vartheta} \wedge \frac{\partial \mathbf{x}}{\partial \psi}. \quad (16)$$

The curvature function can be expressed as a spherical harmonic (Laplace) series

$$G(\vartheta, \psi) = \sum_{l=0}^{\infty} \sum_{m=-l}^l g_{lm} Y_l^m(\vartheta, \psi), \quad 0 \leq \vartheta \leq \pi \quad \text{and} \quad 0 \leq \psi \leq 2\pi \quad (17)$$

where the unnormalized spherical harmonics are

$$Y_l^m(\vartheta, \psi) = P_l^m(\cos \vartheta) e^{im\psi}, \quad (18)$$

P_l^m being an associated Legendre polynomial (see, e.g., [1]). In practical computations, associated Legendre polynomials are most easily generated using their recurrence relations. Since G is a real-valued function, only coefficients g_{lm} , $m \geq 0$, are of interest, the other coefficients being completely determined by these.

Y_{lm} are the basis functions of the irreducible representations of $SO(3)$. We can also use the representations, i.e., the rotation matrices $D_{m'm}^{(l)}$ (see appendix A), as our basis for describing $S^2 \times S^2$ -data. Now the generalized brightness function is [7, 8]

$$L(\omega_0, \omega) = \sum_{lm} g_{lm} \sum_{m'} D_{m'm}^{(l)}(\kappa, \epsilon, \delta) I_{lm'}(\alpha), \quad (19)$$

where the suitably defined Euler angles κ, ϵ, δ and the illumination phase angle α define a point on $S^2 \times S^2$, and

$$I_{lm'}(\alpha) = \int_{\alpha}^{\pi} \int_0^{\pi} S(\mu, \mu_0, \alpha) Y_l^{m'}(\vartheta, \psi) \sin \psi \, d\vartheta \, d\psi. \quad (20)$$

Due to the orthogonality property of $D_{m'm}^{(l)}$, we know that observations at a given α can indeed be written as a series in $D_{m'm}^{(l)}(\kappa, \epsilon, \delta)$. Thus there are always equations directly relating a g_{lm} to an observed D -series coefficient $c_{m'm}^l$. For all l there exist such m' and α that $I_{lm'}(\alpha) \neq 0$, so information on all g_{lm} is preserved in L when $\alpha \neq 0$.

Theorem 1. $S^2 \times S^2$ -data (or actually $S^2 \times S^1$ at least with realistic scattering functions S) uniquely determine the curvature of a convex compact surface.

Remark. Since there are several equations for one g_{lm} , the information content of the data is manifestly more than sufficient for obtaining G . In practice this abundance of information can be used for obtaining the values of additional free physical parameters or to solve for g_{lm} simultaneously from an incomplete data set.

Minkowski [20] has shown that the curvature function G of a convex surface \mathcal{B} uniquely determines its shape \mathbf{x}_B (up to a translation of \mathbf{x}). This so-called Minkowski problem was further discussed by Nirenberg [22].

Corollary. $S^2 \times S^2$ -data uniquely determine the shape of a convex compact surface.

Theorem 2. The mapping $L(\omega_0, \omega) \rightarrow \mathbf{x}_B$ is continuous for convex bodies in usual topologies (the inverse problem is conditionally well posed in the sense of Tikhonov).

The Minkowski proof was translated to a provably convergent numerical solution of the Minkowski problem in the polytope representation in [16] (the outline of this algorithm is discussed in [8]). A solution in function space (Laplace series of the curvature function and support function) was given in [17] (also discussed in [8]). In [10] it was also shown that a measure of the average decrease of generalized projection areas as the phase angle α between ω_0 and ω grows is invariant for convex bodies (with simple scattering functions).

The complete inverse solution chain for photometric data was presented in [9, 10] in a form that manifestly keeps the curvature function positive by an exponential representation. The conditional well-posedness of the problem reveals itself in the fact that, while unconstrained curvature leads to ill-posed behaviour, the positivity constraint is sufficient for keeping the solution stable without additional regularization (we call this Minkowski stability). This formulation allows a general robust optimization algorithm in which we not only reconstruct the shape of the body from photometric data, but also obtain its spin state (rotation vector and period) as well as information on the scattering function. In [11] it was shown that the spin state can be solved also when the object is precessing, i.e., exhibiting a complex rotational state (also known as non-principal-axis rotation).

There is an important ambiguity property for the spin state solution from data obtained in a naturally arising restricted observing geometry. In the following, we prove and discuss this property.

Let $\mathbf{x} = (x, y, z)$ denote a vector in a coordinate system fixed to the target (i.e., rotating with it, the z -axis aligned with the rotation axis), and \mathbf{x}' a vector in a nonrotating system (denoted by primes) where the rotation vector points at the direction given by the spherical coordinates (θ', φ') (rotation is in the positive direction around this vector, with period P). Then \mathbf{x}' and \mathbf{x} are related by

$$\mathbf{x} = \mathbf{R} \mathbf{x}', \quad (21)$$

where

$$\mathbf{R} = \mathbf{R}_z \left(\phi_0 + \frac{2\pi}{P}(t - t_0) \right) \mathbf{R}_y(\theta') \mathbf{R}_z(\varphi'), \quad (22)$$

where t is the time, ϕ_0 and the epoch t_0 are some initial values, and $\mathbf{R}_i(\phi)$ is the rotation matrix corresponding to the rotation of the coordinate frame through angle ϕ counterclockwise about the positive i -axis. In particular, $\mathbf{R}_z(\phi)$ is

$$\mathbf{R}_z(\phi) = \begin{pmatrix} \cos \phi & \sin \phi & 0 \\ -\sin \phi & \cos \phi & 0 \\ 0 & 0 & 1 \end{pmatrix}. \quad (23)$$

Ambiguity theorem. *If the viewing and illumination directions ω' and ω'_0 in a nonrotating frame remain in the same plane at all times of observation t_i , the infinite-distance observations of a body \mathcal{B} , with surface points $\mathbf{b} = (x, y, z)$ and rotation vector $\beta'(\theta', \varphi')$ given in a coordinate system whose equatorial plane is the invariant plane, are indistinguishable from those of a body $\hat{\mathcal{B}}$ with $\hat{\mathbf{b}} = (x, y, -z)$ and $\hat{\beta}' = \beta'(\theta', \varphi' + \pi)$.*

Proof. We choose the invariant plane defined by ω' and ω'_0 as the equatorial plane of the nonrotating system, so the z' -coordinates of the viewer and the illumination source are zero. From (23) we have

$$\mathbf{R}_z(\varphi' + \pi)\mathbf{x}'|_{z'=0} = -\mathbf{R}_z(\varphi')\mathbf{x}'|_{z'=0}, \quad (24)$$

so (22) yields

$$\mathbf{x}(\varphi' + \pi, \mathbf{x}'|_{z'=0}) = -\mathbf{x}(\varphi', \mathbf{x}'|_{z'=0}). \quad (25)$$

Since ϕ_0 is arbitrary, we can set $\hat{\phi}_0 = \phi_0 + \pi$ (as $(x, y) \rightarrow (-x, -y)$ corresponds to a trivial shape rotation of π in the xy -plane). Therefore a vertical mirror-image shape $\hat{\mathcal{B}}$ ($z \rightarrow -z$) with a rotation direction changed by $\varphi' \rightarrow \varphi' + \pi$ has the same viewing and illumination directions with respect to the body shape as \mathcal{B} and thus yields exactly the same observations as those of \mathcal{B} . \square

This ambiguity property affects all data that are not two-dimensionally resolved in a plane projection, i.e., in this sense equivalent to observations made at infinity. Thus it appears also with radar data in addition to photometric observations. The coplanarity of ω' and ω'_0 is a case often approximated in the solar system as many targets move close to the plane of the Earth's orbit around the Sun. For such targets, only observations with resolved plane-of-sky projections can properly remove the spin direction ambiguity.

In [10, 14, 19], it was shown by numerical simulations as well as with known space and laboratory targets that the convex inversion gives a good representation of a target \mathcal{B} of any shape (unless it is extremely far away from a convex shape), typically close to its convex hull, and that the result is not sensitive to the incorrectness of the scattering model S . Furthermore, Āurech and Kaasalainen [2] showed that disc-integrated photometry does not contain extractable information on nonconvex features of the target unless these are very large (relative to the target's size) and the phase angle α is large. They derived an approximate linear relationship between α and the minimal required value of nonconvexity volume \mathcal{V}_{nc} , a measure of the nonconvexity of the target. A type of convex representation was also discussed in [23], where it was studied whether it is possible to extract some shape information about the target from a strongly limited and minimal photometric data set in the form of an average cross section.

Finally, to conclude the century-long historical list of photometric inversion, we note that in [12] it was shown that even when the spin state of the object is unknown, a time series of photometric data with sampling intervals much longer than the rotation period is still sufficient for solving both the spin state and the shape. This underlines the fact that the mathematical model imposes strict constraints on the solution, allowing considerably sparser time sampling than required for non-modelling time-series methods based on frequency analysis.

4. Radar operator

Here we address mainly the theoretical fundamentals of the problem. Numerical procedures for solving radar inverse problems of this kind are well known and widely used for planetary targets in practice (this technique was pioneered by Ostro; see [24] and the numerous references

therein). Our aim is to point out some properties of the inverse problem and to introduce a compact formulation that utilizes the intrinsic rotational symmetries of the observation geometries. In our analysis, we use a spherical harmonics series for a continuous representation of the surface reflectivity. In contrast to, e.g., [6], we use the rotational properties of spherical harmonics since the analysis requires rotational coordinate transforms. These properties make the formulation of the problem very compact and efficient.

It can easily be seen that we have to confine ourselves to targets whose shape is known in order to obtain a provably unique solution for the inverse problem: if the shape is unknown, the problem becomes strongly nonlinear and is no longer analytically tractable. In this section, the target is taken to be spherical since this makes a compact and useful formulation possible. In this way we can prove uniqueness theorems for inverse problems of radar data corresponding to generalized projection operators; to our knowledge, no such theorems have been proved before. The sphere is also a shape often encountered in practice as many planetary targets are spherical.

By spherical radar inverse problem, we mean the problem of obtaining information on the reflectivity function(s) and scattering function(s) of a spherical target with radar-type projection operators. The radius of the sphere is chosen as the unit of distance, and the reflectivity function is described by ρ . When referring to a point on the sphere, we use spherical polar coordinates (ϑ, ψ) . Analogously to the curvature function in the photometric case, the reflectivity function can be expressed as a Laplace series

$$\rho(\vartheta, \psi) = \sum_{l=0}^{\infty} \sum_{m=-l}^l \varrho_{lm} Y_l^m(\vartheta, \psi), \quad 0 \leq \vartheta \leq \pi \quad \text{and} \quad 0 \leq \psi \leq 2\pi. \quad (26)$$

4.1. $\mathcal{P}(\omega, d)$ and the inverse solution

The range-dimension case is best studied with two coordinate systems. The rectangular system (x, y, z) rotates with the sphere such that the z -axis coincides with the rotation axis, while a coordinate system (x_r, y_r, z_r) is oriented such that the positive z_r axis always points towards the radar. In the latter system, iso- d contours are thus concentric rings around the radar direction ω , and $\mu = \cos \vartheta_r = z_r = d$, $-1 \leq d \leq 1$, so the scattering function is expressed by $S(d)$. Since the reflectivity function in (26) is expressed as a function of the spherical coordinates in the system (x, y, z) , we must rotationally transform this function to calculate the projection integral in the system (x_r, y_r, z_r) . This is done by using the rotational properties of spherical harmonics. If P_R is an operator transforming a function in any arbitrary rotation $R(\gamma, \beta, \alpha)$ (α operating first), we have

$$P_R(\gamma, \beta, \alpha) Y_l^m(\vartheta, \psi) = \sum_{m'=-l}^l Y_l^{m'}(\vartheta, \psi) D_{m'm}^{(l)}(\gamma, \beta, \alpha) \quad (27)$$

(for a description of $D_{m'm}^{(l)}$ see appendix A).

By setting the Euler angles to

$$\alpha = \varphi \quad \beta = \theta \quad \gamma = 0, \quad (28)$$

where θ and φ are as in (8), we perform the rotation $(x, y, z) \rightarrow (x_r, y_r, z_r)$ and thus have L (as a density function of power per an infinitesimal width of d)

$$L(\theta, \varphi, d) = S(d) \int_0^{2\pi} \rho(\vartheta, \psi) d\psi = 2\pi S(d) \sum_{lm} \varrho_{lm} \sum_{m'} D_{m'm}^{(l)}(0, \theta, \varphi) P_l^{m'}(d) \delta_{m'0}, \quad (29)$$

so, using the identity (appendix A)

$$Y_l^m(\vartheta, \psi) \equiv D_{0m}^{(l)}(0, \vartheta, \psi), \quad (30)$$

we obtain

$$L(\theta, \varphi, d) = 2\pi S(d) \sum_{lm} P_l(d) \varrho_{lm} Y_l^m(\theta, \varphi), \quad (31)$$

where P_l are Legendre polynomials.

Uniqueness theorem 1. Complete $\omega \in S^2$ and range coverage $0 \leq d \leq 1$ of $L(\omega, d)$ of a unit sphere uniquely determines (up to an arbitrary multiplicative constant) both its reflectivity function $\rho(\omega)$ and scattering function $S(\mu)$.

Proof. If observations are given as

$$L_{\text{obs}}(\theta, \varphi, d) = \sum_{lm} a_{lm}(d) Y_l^m(\theta, \varphi) \quad (32)$$

(a_{lm} can be a function series in d or equivalent), we can then define coefficients b_{lm} as

$$\frac{a_{lm}(d)}{P_l(d)} := b_{lm} F(d) \quad (33)$$

with the condition that $F(d)$ be the same for all lm (at those d for which $P_l(d) = 0$ or $S(d) = 0$, of course $a_{lm}(d) = 0$ in our model, so such points represent no singularities). For example, we can choose $b_{00} = 1$, so $b_{lm} = a_{lm}(d)/[a_{00}(d)P_l(d)]$. Thus we can write

$$L_{\text{obs}} = F(d) \sum_{lm} b_{lm} Y_l^m(\theta, \varphi) P_l(d), \quad (34)$$

i.e., we immediately have

$$\varrho_{lm} = \frac{b_{lm}}{2\pi} \quad (35)$$

and we directly obtain the scattering function $S(\mu) = F(d)$. \square

Remark. More complex forms of the scattering function are also possible. For example, instead of one $S(\mu)$, we may have a linear combination of several independent $S_i(\mu)$, each coupled to their own reflectivity function over the sphere. The projection operator kernel is now of the form

$$P = \sum_i S_i(\mu) \rho_i \, d\sigma. \quad (36)$$

Thus we have

$$L(\theta, \varphi, d) = 2\pi \sum_i S_i(d) \sum_{lm} P_l(d) \varrho_{lm}^{(i)} Y_l^m(\theta, \varphi), \quad (37)$$

and now

$$\frac{a_{lm}(d)}{P_l(d)} := \sum_i b_{lm}^{(i)} F_i(d), \quad (38)$$

where we can expand the observed left-hand side with, e.g., any suitable orthogonal polynomials F_i , and define these polynomials and their weights to be the scattering functions and the coefficients of the corresponding Laplace series for reflectivity functions.

Corollary. Complete $L(\omega, d)$ -data solve the spherical radar inverse problem completely, yielding all the unknown parameters of reflectivity and scattering functions.

4.2. $\mathcal{P}(\omega, \mathcal{D})$ and the inverse solution

Transmitting a continuous wave (CW) signal to a rotating target and measuring the echo power at different Doppler frequencies is a particularly simple radar experiment to perform. Thus it is of interest to study theoretically the possibilities and limitations of this technique.

As before, we use two coordinate systems sharing a common origin at the sphere’s centre. However, now the y_r axis coincides with the direction of the radar and the z_r axis lies in the equator plane of the sphere. The coordinate system (x_r, y_r, z_r) is obtained from the system (x, y, z) by the Euler angles

$$\alpha = \pi/2 + \varphi \quad \beta = \pi/2 \quad \gamma = \pi/2 + \theta. \tag{39}$$

By the definition of the coordinate system (x_r, y_r, z_r) we have $\mu = y_r$, and the Doppler frequency D is correspondingly now written as $D = -wz_r \sin \theta$, where the positive constant w depends on the rotational velocity of the sphere, so now we have $\hat{D} = -z_r = -\cos \vartheta, -1 \leq \hat{D} \leq 1$ (ϑ and ψ referring now to the coordinate system (x_r, y_r, z_r)). The observed echo power $L(\theta, \varphi, \mathcal{D})$ at a fixed Doppler frequency is obtained by taking a line integral along the ‘visible stripe’ $\cos \vartheta = -\hat{D} = \text{constant}$ and is thus (expressed as a density function per $d\hat{D} = \sin \vartheta d\vartheta$)

$$L(\omega, \mathcal{D}) = \int_0^\pi \rho(\vartheta, \psi) S(y_r) d\psi. \tag{40}$$

Our problem is to solve the function ρ from this integral equation.

If we assume that $S = y_r^n, n > -1, n \in \mathbb{R}$, we can, using the rotational transform and

$$y_r = \sin \vartheta \sin \psi = (1 - \cos^2 \vartheta)^{\frac{1}{2}} \sin \psi = (1 - \hat{D}^2)^{\frac{1}{2}} \sin \psi, \tag{41}$$

write (40) as

$$\begin{aligned} L(\omega, \mathcal{D}) &= (1 - \hat{D}^2)^{\frac{n}{2}} \int_0^\pi \rho(\vartheta, \psi) \sin^n \psi d\psi \\ &= (1 - \hat{D}^2)^{\frac{n}{2}} \sum_l \sum_{m=-l}^l \varrho_{lm} \sum_{m'=-l}^l D_{m'm}^{(l)}(\gamma, \beta, \alpha) P_l^{m'}(-\hat{D}) I_{m'}^n, \end{aligned} \tag{42}$$

where

$$I_{m'}^n = \int_0^\pi e^{im'\psi} \sin^n \psi d\psi. \tag{43}$$

If n is an integer, $I_{m'}^n$ can be computed in a closed form. In the case $m' + n$ is an even integer and $|m'| \leq n$,

$$I_{m'}^n = \pi \left(\frac{1}{2i}\right)^n (-1)^{\frac{m'+n}{2}} \binom{n}{\frac{m'+n}{2}}. \tag{44}$$

If $m' + n$ is even and $|m'| > n$, $I_{m'}^n$ vanishes (and, what is more, $I_{m'}^n$ vanishes only in this case, as is shown in appendix B). If $m' + n$ is odd,

$$I_{m'}^n = \left(\frac{1}{2i}\right)^{n-1} \sum_{k=0}^n (-1)^k \frac{\binom{n}{k}}{m' + n - 2k}. \tag{45}$$

Using (A.4) and (39) we can write (42) in the form

$$L(\theta, \varphi, \mathcal{D})(1 - \hat{D}^2)^{-\frac{n}{2}} = \sum_l \sum_{m=-l}^l \varrho_{lm} \sum_{m'=-l}^l k_{m'm}^{(l)n} P_l^{m'}(-\hat{D}) e^{i(m'\theta+m\varphi)}, \tag{46}$$

where

$$k_{m'm}^{(l)n} = e^{i(m+m')\pi/2} I_m^n d_{m'm}^{(l)}(\pi/2), \tag{47}$$

$d_{m'm}^{(l)}$ being described in appendix A. Thus we have written the integral equation (42) in a new form; the measured quantity is on the left-hand side and the function to be obtained, represented by the coefficients q_{lm} , is to be extracted from the right-hand side. If we have complete coverage of $L(\theta, \varphi, \mathcal{D})$ in the $(\theta, \varphi, \hat{\mathcal{D}})$ -space, we can use the orthogonality properties of the functions P_l^m and $e^{i(\cdot)}$:

$$\int_0^{2\pi} e^{-im\varphi} e^{ik\varphi} d\varphi = 2\pi \delta_{mk}, \quad \int_{-1}^1 P_l^m(-\hat{\mathcal{D}}) P_k^m(-\hat{\mathcal{D}}) d\hat{\mathcal{D}} = \frac{2}{2l+1} \frac{(l+m)!}{(l-m)!} \delta_{lk}, \tag{48}$$

$(m, k, l \in \mathbb{Z})$ so that

$$\begin{aligned} & \frac{8\pi^2}{2l+1} \frac{(l+m')!}{(l-m')!} k_{m'm}^{(l)n} q_{lm} \\ &= \int_0^{2\pi} \int_0^{2\pi} \int_{-1}^1 L(\theta, \varphi, \mathcal{D}) (1 - \hat{\mathcal{D}}^2)^{-\frac{n}{2}} P_l^{m'}(-\hat{\mathcal{D}}) e^{-i(m'\theta+m\varphi)} d\hat{\mathcal{D}} d\theta d\varphi \end{aligned} \tag{49}$$

for all $-l \leq m' \leq l$. On the right-hand side, the range of θ is $[0, 2\pi]$; this can be formally accomplished using $L(\theta, \varphi, \mathcal{D}) = L(2\pi - \theta, \varphi + \pi, -\mathcal{D})$. In practice, the integral over θ means that L can be expressed as a Fourier series in θ .

If at least one m' , $-l \leq m' \leq l$, can be found, for which $k_{m'm}^{(l)n} \neq 0$, the coefficient q_{lm} can be solved; below we will show that this is indeed the case. It is also interesting to note that because (49) usually provides many equations for an unknown coefficient q_{lm} , the amount of information available is more than needed for the determination of the coefficients. This case thus resembles the photometric one discussed in [7, 8].

The series describing the reflectivity function does not have to be truncated *a priori*: the accuracy and density of the observations determine to which degree l and order m the right-hand side of (49) can be computed. However, for planetary targets the coverage of the subradar latitude θ is seldom sufficient for even a crude estimate for the integral in (49), i.e., for the Fourier series of the reflectivity function in θ . This means that the unknown coefficients must be solved by linear sets of equations through (46). Again, this is analogous to the photometric case, particularly as regards the regularization of ill-posedness. This approach is also necessary if the scattering function is more complex than the simple power function here. However, it is interesting to note that if the scattering function is of the form $S = \rho_1 \mu^n + \rho_2 \mu^p$ where $p \neq n$ and the difference between p and n is an integer, a solution analogous to (49) can be obtained using the orthogonality relations and the recurrence relations for associated Legendre polynomials.

The main difference between the radar case and the photometric one is that the latter can be studied via the Gaussian image sphere (the S^2 -mapping encompasses radii of convex shapes in \mathbb{R}^3), while in the former no such mapping is available as d and \mathcal{D} are directly related to the spatial dimensions of the target, so we are restricted to the sphere directly in \mathbb{R}^3 in our uniqueness theorems.

We now prove the uniqueness of the Doppler-radar solution. Let l and m be fixed. We will show that $k_{m'm}^{(l)n} \neq 0$ at least for one value of index m' , $-l \leq m' \leq l$. In what follows we will use the following lemma, proved in appendix B.

Lemma. *Let $n > -1$ and $m' \in \mathbb{R}$. The integral I_m^n is zero when and only when $|m'| = n + 2k, k = 1, 2, 3, \dots$*

Uniqueness theorem 2. *Let $n > -1, l = 0, 1, \dots$ and $-l \leq m \leq l$. Among the coefficients $k_{m'm}^{(l)n}$ in (47) there is at least one nonzero. Hence three-dimensional $(\theta, \varphi, \mathcal{D})$ -data determine the reflectivity function ρ uniquely.*

Proof. Let l and m be fixed. If $l+n$ is not an even integer, we choose $m' = l$. According to the lemma and (A.7) $I_l^n \neq 0$ and $d_{lm}^{(l)}(\pi/2) = \frac{(-1)^{l-m}}{2^{l-m}} \neq 0$, so $k_{lm}^{(l)n} \neq 0$.

If $l+n$ is an even integer, we choose $m' = l-1$ ($l > 0; k_{00}^{(0)n} \neq 0; I_{l-1}^n \neq 0$). It can easily be seen by inspection from (A.7) that $d_{(l-1)m}^{(l)}(\pi/2) = 0$ only when $m = 0$ and thus $k_{(l-1)m}^{(l)n} \neq 0$ when $m \neq 0$. If $m = 0$ we can write using (A.8)

$$d_{m'0}^{(l)}(\pi/2) = d_{0(-m')}^{(l)}(\pi/2) = D_{0(-m')}^{(l)}(0, \pi/2, 0) = Y_l^{-m'}(\pi/2, 0) = P_l^{-m'}(0). \quad (50)$$

As is well known, $P_l^k(0) \neq 0$ when $l+k$ is even (e.g., [1]). If l is even, we can choose $m' = 0$; if it is odd, we choose $m' = 1$. In both cases $d_{m'0}^{(l)}(\pi/2) \neq 0$ and $|m'| \leq n+1$; thus, taking the lemma into account, it is directly seen that $I_{m'}^n \neq 0$. Therefore $k_{m'm}^{(l)n} \neq 0$. \square

Remark on information content. In addition to establishing the uniqueness of the inverse solution, it is interesting to examine how small data sets still fulfil a uniqueness property. For this purpose, (46) has the special property of being a sum over three indexed functions and variables, while the orthogonality properties of two functions pertaining to a pair of indices are already sufficient to yield uniquely solvable equations for q_{lm} with any given l , if the scattering function is suitable. In appendix C we show that if $S = \mu^n, n > -1$, and $n \in \mathbb{R}$ is not an integer, two-dimensional $L(\theta, \mathcal{D})$ -data corresponding to any fixed phase φ_0 already determine the reflectivity function ρ uniquely. This underlines the importance of coverage in the polar angle θ .

The above discussion of the properties of Doppler-resolution, together with the fact that range-resolution radar data already completely solve the spherical radar problem, underlines the fact that it is the range-resolution possibility of radar experiments that carries the most part of the crucial additional information that makes radar observations so powerful. Simultaneous range- and Doppler-resolution offers even more information obtainable with numerical routines [24]. This case can be written as a straightforward extension of the $\mathcal{P}(\omega, d)$ -formulation via the examination of the surface patches of the $d = \text{const}$ -circle intersected by the $\hat{D} = \text{const}$ -stripe, but this introduces no obviously useful additional analytical properties relevant to the analysis here. In fact, infinitesimal surface patches of this kind are ill-defined on the part of the surface where the \hat{D} -stripe is tangent to the d -circle, i.e., when $\hat{D}^2 + d^2 = 1$. Patches close to this region are very different in relative size and shape from those in the region where the stripe is normal to the circle, so in this sense $(D + \Delta D, d + \Delta d)$ -patches sample the surface unevenly.

5. Multidatoinversion with generalized projection operators

Since there are many observing modes of a target body, corresponding to various types of projection operators, a natural application is to use these data simultaneously to obtain the best estimates of the parameters modelling the target. We call this multidatoinversion. A typical combination in astrophysics is that of photometry together with one or more complementary sources. Here we present examples of two such combinations. Typically, photometry already provides a good estimate of the parameters, and the complementary source is employed to yield a detailed solution; most often the improvement lies in revealing nonconvex features of the body or in removing the spin solution ambiguity discussed above.

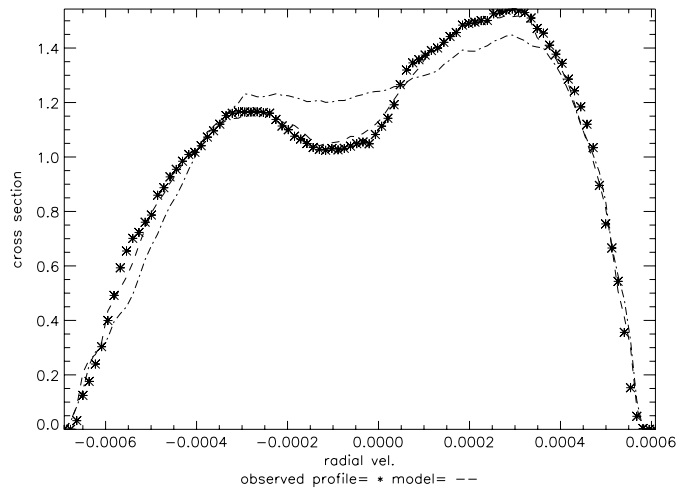


Figure 1. Doppler spectrum of the target (asterisks), with fits from convex model based on photometry alone (dot-dashed line) and the nonconvex model based on combined photometry and radar (dashed line).

The general principle of multidatainversion is to form a joint goodness-of-fit χ_{tot}^2 that combines the χ^2 from the main source with the χ_i^2 of the complementary sources i , multiplied by suitable weights λ_i . Thus we have

$$\chi_{\text{tot}}^2 = \chi^2 + \sum_i \lambda_i \chi_i^2. \quad (51)$$

The weights are adjusted in minimizing χ_{tot}^2 with the condition that each χ_i^2 as well as χ^2 be acceptable. This condition usually leads to a certain degree of nonuniqueness in the solution as there may be several feasible sets of weights that fulfil the condition and lead to virtually equal values of χ_{tot}^2 . Also, the exact values of the maximal allowed χ_i^2 are usually not well defined in practice: these depend not only on the noise levels of the individual sources, but also on systematic effects such as the expected reliability of a source. Furthermore, insufficiency of the model affects fits for separate data sources differently. In practice, the multidatainversion results from generalized projection operators appear to be quite stable; one reason for this is the stability of the solution from the main source, photometry.

5.1. CW radar and photometry

Here we demonstrate the important role of even small data sets of complementary information in multidatainversion. In figure 1 we show the simulated Doppler spectrum (in arbitrary units) of the target on the left in figure 2. The viewing direction ω is the same in both cases (note that the sign convention of the Doppler velocity \mathcal{D} makes the spectrum look like a ‘mirror image’). The convex inversion of simulated photometric data produces a model close to the convex hull of the target, giving an excellent fit to the data [9, 10]. Thus the data do not contain proper information on the sizable nonconvex features of the target (cf [2, 14]). However, the convex model gives a poor fit to the observed Doppler spectrum (dot-dash line), so even one spectrum already contains significant information when added to other data. Using a Laplace series for the radius of the (starlike) model [9, 10] and the Levenberg–Marquardt algorithm to minimize the χ_{tot}^2 [25], we obtained the nonconvex model displayed on the right in figure 2. The generalized projection integrals were computed with a densely tessellated

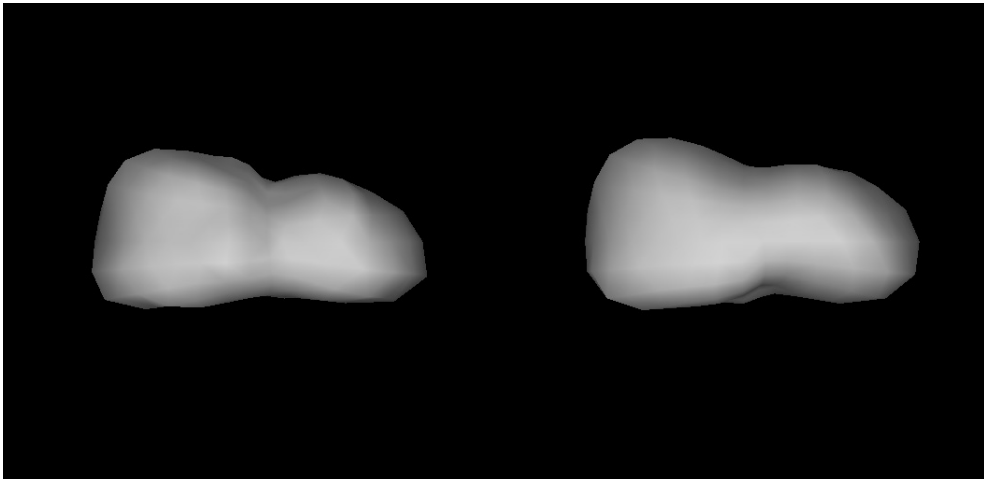


Figure 2. View of the target (left) and the nonconvex model (right) in the same direction ω in which the Doppler spectrum was computed.

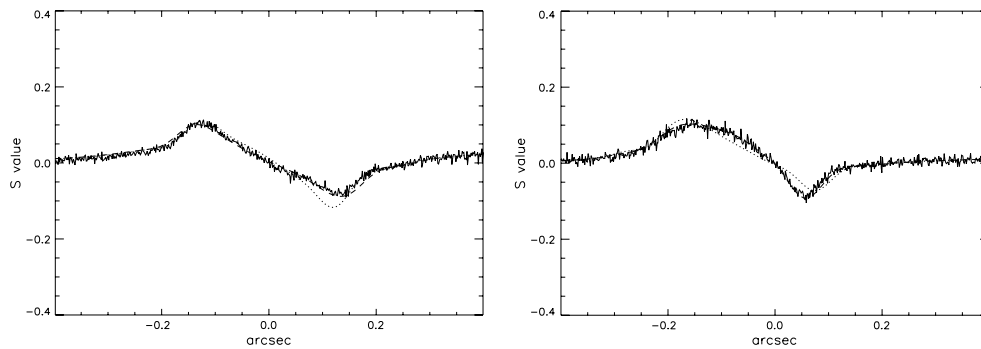


Figure 3. Two examples of interferometric curves (solid line) measured for asteroid Eunomia in different geometries. The fit from the photometry-based convex model is shown with a dotted line, and that from combined photo- and interferometric model with a dashed line.

polyhedral surface representation [9]. While still giving an excellent fit to photometric data, the model also fits the Doppler spectrum very well (dashed line), and well reproduces the main features of the target (with lower resolution: $\max l, m = 6$ for the Laplace series).

5.2. Interferometry and photometry

Interferometric observations of solar system targets can be obtained with many ground-based and space telescopes; here we show a result for interferometric Hubble Space Telescope data of asteroid 15 Eunomia [5] combined with photometry [21]. The interferometer divides the incident wavefront into two, each half is split into a reflected component and a transmitted phase-retarded component, and these components are made to interfere with each other in two different combinations, yielding convolved projections (discussed in section 2.4) in two orthogonal directions. The data set consisted of 31 lightcurves (photometric time series of a few hours) and 18 interferometric curves measured at various geometries. Two examples of the latter are shown in figure 3. The abscissae give the measurement coordinate length s

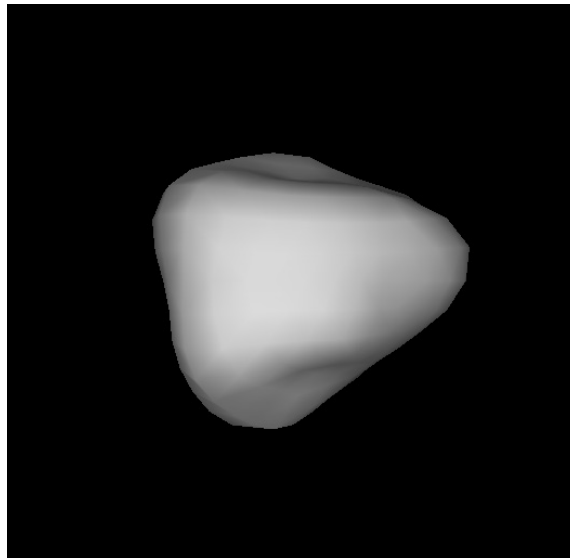


Figure 4. Equatorial view of the multidata inversion model of Eunomia.

on a great circle S^1 in arcseconds, plotted against the normalized so-called S -value, the value from the operator (11) divided by $L(\omega_0, \omega)$. Again, the prediction of the convex model from photometry alone (dotted line) deviates somewhat from the observations, but the model from combined photo- and interferometry gives an excellent fit (dashed line). The model shape, shown in figure 4, displays some nonconvex features, but otherwise is consistent with the convex model of [21], with virtually the same solutions for spin vector direction and rotation period.

6. Conclusions and discussion

We have introduced the family of generalized projection operators, and reviewed and discussed their typical properties and related inverse problems. These operators and inverse problems appear very naturally in many cases of physical observations with various instruments. Photometry and radar have proved to be particularly important in planetary studies; their robustness as data sources is corroborated by strong uniqueness theorems and stability properties.

The radar observables described here are a kind of idealization of the real physical case. In this setup, the echo power for separate (d, \mathcal{D}) -bins is obtained by computing the (Fourier) power spectrum (a function of \mathcal{D}) of the received Doppler-dispersed signal at very small time intervals corresponding to each d -bin. Such an experiment requires a very powerful radar, so real observations are usually very noisy particularly for faraway targets. One possibility is to use suitable varying pulse sequences for the radar signal such that various combinations of range distances are simultaneously observed by the radar—this increases the echo signal strength while still allowing the disentangling of different d -regions (cf [18]). However, a more fundamental point is that the obtained $L(d, \mathcal{D})$ is not a function of the actual physical observable, i.e., the time series of the voltage amplitude received by the antenna. From the mathematical point of view, the radar inverse problem should ideally be formulated in the

amplitude/time domain instead of the power/frequency domain. This, of course, requires large storage capacity and high computing speed for proper numerical solution. Initial experiments with such equipment are described in, e.g., [18]. Also, the physical scattering model is more difficult to describe in the amplitude domain than in the traditional power formulation. One possibility for practical time-domain formulation is to use the Itô measure to represent the stochastically scattering material in order to properly take into account the incoherent summation of amplitudes $|A + B|^2 \rightarrow |A|^2 + |B|^2$ (in power domain included in the projection integral and power-scattering law S). In this case, we would analyse integrals of the form (supposing a stationary target)

$$e(t) = \int \int_{A^+} \tilde{S}(\mu) e^{i2\pi f[t-2R(\mathbf{x})/c]} \zeta(d\sigma(\mathbf{x})) \quad (52)$$

for a large number of epochs t_i . Here e is the observed voltage, R is the distance to the radar, c is the speed of light, f is the transmission frequency, \tilde{S} is the amplitude scattering model and ζ is the stochastic measure. This formulation is obviously quite different from the power/frequency case that can be understood via generalized projection formalism.

Multidatoinversion can be performed with a wide variety of data modes. In astrophysics, a complementary data source closely related to generalized projection operators is astrometry, i.e., the accurate measurement of the location of the brightness centroid of the target's projection on the plane-of-sky S^2 . We can say that, for Ω on this S^2 , this corresponds to the kernel (cf equation (13))

$$P(\omega_0, \omega, \Omega) = \Omega' S(\mu_0, \mu, \alpha) \rho / L(\omega_0, \omega). \quad (53)$$

Combined with photometry, the full inverse problem for this data mode yields the shape and spin state of a planetary target as well as its accurate orbit [13].

The fundamental problem in multidatoinversion is the determination of the weights λ_i . The intuitively clear method of section 5 is obviously not rigorously defined, so it is natural to ask whether one could define an exact optimization process, where the factors λ_i are determined simultaneously with the model parameters. This requires an objective function different from the joint χ_{tot}^2 , allowing the optimization of λ_i . One possibility for this is spline estimation with smoothing multiparameters in reproducing kernel Hilbert spaces [27]. This allows the definition of an objective function $V(\lambda)$ with ordinary or general cross-validation testing and suitable penalty functionals. We plan to report on this approach in a future paper.

To wind up, we note an interesting phenomenon regarding the stability properties of photometric inversion. On conjectural level, it appears that the purely photometric $L(\omega_0, \omega)$ -data of at least a starlike nonconvex body (at least when observed at phase angles α sufficiently high) determine its shape as robustly as with a convex body, but *only if* the scattering function is known accurately and the noise level is low [2, 10]. In all simulations we have carried out, a nonconvex model efficiently converges towards the correct minimum of χ^2 , faithfully displaying the same features as the target even with model resolution (discretization of the problem) much lower than that of the simulation model. This seems to be a mathematically interesting extension of the uniqueness theorem for convex bodies. However, accurate photometry of real targets of known nonconvex shapes but with inadequately known (and modelled) scattering functions does not yield similar convergence. This is an example of how taking the numerical conjecture directly as a model of reality would be an 'inverse crime' [15] leading to overoptimistic results: nonconvex photometric inversion is sensitive to the insufficiency of the scattering model, and in reality the scattering behaviour is never known well enough for this purpose. On the other hand, due to Minkowski stability, *convex* inversion is quite stable against the incorrectness of the scattering law [10, 14, 16].

Acknowledgments

It is our pleasure to thank Markku Lehtinen and Lassi Päiväranta as well as the anonymous referees for valuable discussions and comments; ML, Sodankylä Geophysical Observatory, and Arctic Research Centre of the Finnish Meteorological Institute for hospitality during MK's stay in Sodankylä where part of this work was carried out; and Daniel Hestroffer for the sample interferometric data from the Hubble Space Telescope. This work was supported by Academy of Finland grant no 112018.

Appendix A. Euler angles, spherical harmonics and rotation matrices

All rotations in the three-dimensional space can be parametrized by Euler angles, which are here defined as follows: the rotation $R(\gamma, \beta, \alpha)$ of a coordinate system involves three successive rotations:

- (1) A rotation through angle α about the z -axis in the positive rotation direction.
- (2) A rotation through angle β about the new y -axis in the positive rotation direction.
- (3) A rotation through angle γ about the newest z -axis in the positive rotation direction.

After rotating a coordinate system, the functions expressed in this system must be transformed accordingly in such a way that their values will remain unchanged; thus, when a vector \mathbf{x} is transformed as

$$\mathbf{x} \rightarrow \mathbf{x}', \quad \mathbf{x}' = R\mathbf{x}, \quad (\text{A.1})$$

where R is the operator performing the rotation, the value of a scalar function f in a point in space must remain unchanged. Thus

$$f'(\mathbf{x}') = f(\mathbf{x}), \quad (\text{A.2})$$

where $f'(\mathbf{x}')$ is the function in the new coordinate system. Satisfying this condition, spherical harmonics transform under the rotation $R(\gamma, \beta, \alpha)$ as

$$Y_l^m(\vartheta, \psi) = \sum_{m'=-l}^l Y_l^{m'}(\vartheta, \psi) D_{m'm}^{(l)}(\gamma, \beta, \alpha), \quad (\text{A.3})$$

where Y_l^m is the form of the function in the new coordinate system, and the element $D_{m'm}^{(l)}$ of a rotation matrix $D^{(l)}$ is (see, e.g., [1, 28]; note the difference in the normalization convention)

$$D_{m'm}^{(l)}(\gamma, \beta, \alpha) = e^{im'\gamma} d_{m'm}^{(l)}(\beta) e^{im\alpha} \quad (\text{A.4})$$

where

$$d_{m'm}^{(l)}(\beta) = \sum_{\lambda=0}^{l+m} C_{m'm}^{(l)\lambda} \left(\cos \frac{\beta}{2} \right)^{2l+m-m'-2\lambda} \left(\sin \frac{\beta}{2} \right)^{m'-m+2\lambda} \quad (\text{A.5})$$

and

$$C_{m'm}^{(l)\lambda} = \frac{(-1)^{\lambda+m'-m} (l+m)! (l-m')!}{\lambda! (l+m-\lambda)! (l-m'-\lambda)! (m'-m+\lambda)!}. \quad (\text{A.6})$$

A term in the sum vanishes if an argument of a factorial in the denominator is negative. If $\beta = \pi/2$, we have

$$d_{m'm}^{(l)}(\pi/2) = 2^{-l} \sum_{\lambda=0}^{l+m} C_{m'm}^{(l)\lambda}. \quad (\text{A.7})$$

A relation between spherical harmonics and the elements of the rotation matrices is

$$Y_l^m(\vartheta, \psi) = D_{0m}^{(l)}(0, \vartheta, \psi). \quad (\text{A.8})$$

Appendix B. Proof of the lemma

First we examine the integral $I_{m'}^n$ (43) more closely. Integrating by parts the result

$$I_{m'}^n = \frac{(n+2)^2 - m'^2}{(n+1)(n+2)} I_{m'}^{n+2} \quad (\text{B.1})$$

($n > -1$) is obtained. Thus, by induction,

$$I_{m'}^n = \prod_{k=1}^N \frac{(n+2k)^2 - m'^2}{(n+2k-1)(n+2k)} I_{m'}^{n+2N} \quad (\text{B.2})$$

for every $N = 1, 2, 3, \dots$. Next, two auxiliary lemmas are needed.

Lemma A. *Let $n \geq |m'|$. Then*

$$\prod_{k=1}^{\infty} \frac{(n+2k)^2 - m'^2}{(n+2k)^2} > 0. \quad (\text{B.3})$$

Proof. Since the sequence $\left\{ \prod_{k=1}^N \frac{(n+2k)^2 - m'^2}{(n+2k)^2} \right\}_{N=1,2,3,\dots}$ is decreasing and it has a lower limit zero, the limit exists and it is at least zero. Using the Taylor expansion of the function \ln we have

$$\begin{aligned} \ln \frac{(n+2k)^2 - m'^2}{(n+2k)^2} &= \ln \left[1 - \frac{m'^2}{(n+2k)^2} \right] \\ &\geq -\frac{m'^2}{(n+2k)^2} \left[1 - \frac{m'^2}{(n+2k)^2} \right]^{-1} \geq -2 \frac{m'^2}{(n+2k)^2}, \end{aligned} \quad (\text{B.4})$$

when k is sufficiently large. Thus

$$\ln \prod_{k=1}^N \left[1 - \frac{m'^2}{(n+2k)^2} \right] \geq -2 \sum_{k=1}^N \frac{m'^2}{(n+2k)^2} \quad (\text{B.5})$$

and since the series on the right-hand side is convergent as $N \rightarrow \infty$, we obtain

$$\ln \prod_{k=1}^{\infty} \left[1 - \frac{m'^2}{(n+2k)^2} \right] = \lim_{N \rightarrow \infty} \ln \prod_{k=1}^N \left[1 - \frac{m'^2}{(n+2k)^2} \right] > -\infty. \quad (\text{B.6})$$

□

Lemma B. *The limit exists and*

$$\lim_{N \rightarrow \infty} \prod_{k=1}^N \frac{n+2k}{n+2k-1} I_{m'}^{n+2N} = e^{im'\pi/2} I_0^n = e^{im'\pi/2} \int_0^\pi \sin^n \phi \, d\phi. \quad (\text{B.7})$$

Proof. First, $\prod_{k=1}^N \frac{n+2k}{n+2k-1} < \frac{n+2N}{n+1}$. Second,

$$\int_0^\pi \sin^n \phi \, d\phi = I_0^n = \prod_{k=1}^N \frac{n+2k}{n+2k-1} I_0^{n+2N} = \prod_{k=1}^N \frac{n+2k}{n+2k-1} \int_0^\pi \sin^{n+2N} \phi \, d\phi. \quad (\text{B.8})$$

Let $\epsilon > 0$. We can find $\phi_\epsilon \in]0, \pi/2[$ such that $|e^{im'\pi/2} - e^{im'\phi}| \leq [\int_0^\pi \sin^n \phi \, d\phi]^{-1} \frac{\epsilon}{2}$, when $|\pi/2 - \phi| \leq \phi_\epsilon$.

$$\begin{aligned} \left| e^{im'\pi/2} I_0^n - \prod_{k=1}^N \frac{n+2k}{n+2k-1} I_{m'}^{n+2N} \right| &\leq \prod_{k=1}^N \frac{n+2k}{n+2k-1} \left| \int_0^\pi (e^{im'\pi/2} - e^{im'\phi}) \sin^{n+2N} \phi \, d\phi \right| \\ &\leq \prod_{k=1}^N \frac{n+2k}{n+2k-1} \frac{\epsilon}{2} \left[\int_0^\pi \sin^n \phi \, d\phi \right]^{-1} \int_{\pi/2-\phi_\epsilon}^{\pi/2+\phi_\epsilon} \sin^{n+2N} \phi \, d\phi \\ &\quad + \prod_{k=1}^N \frac{n+2k}{n+2k-1} \left[\int_0^{\pi/2-\phi_\epsilon} 2 \sin^{n+2N} \phi \, d\phi + \int_{\pi/2+\phi_\epsilon}^\pi 2 \sin^{n+2N} \phi \, d\phi \right] \\ &\leq \frac{\epsilon}{2} \left[\int_0^\pi \sin^n \phi \, d\phi \right]^{-1} \int_0^\pi \sin^n \phi \, d\phi + 2\pi \frac{n+2N}{n+1} \cos^{n+2N} \phi_\epsilon. \end{aligned} \tag{B.9}$$

Since $\cos \phi_\epsilon < 1$, $\lim_{N \rightarrow \infty} (n+2N) \cos^{n+2N} \phi_\epsilon = 0$. Thus, when N is sufficiently large,

$$\left| e^{im'\pi/2} I_0^n - \prod_{k=1}^N \frac{n+2k}{n+2k-1} I_{m'}^{n+2N} \right| \leq \epsilon. \tag{B.10}$$

□

Using these results we can prove our final lemma.

Lemma. *Let $n > -1$ and $m' \in \mathbb{R}$. The integral $I_{m'}^n$ is zero when and only when $|m'| = n + 2k, k = 1, 2, 3, \dots$*

Proof. According to (B.2)

$$\begin{aligned} I_{m'}^n &= \prod_{k=1}^N \frac{(n+2k)^2 - m'^2}{(n+2k-1)(n+2k)} I_{m'}^{n+2N} \\ &= \prod_{k=1}^N \frac{(n+2k)^2 - m'^2}{(n+2k)^2} \prod_{k=1}^N \frac{n+2k}{n+2k-1} I_{m'}^{n+2N}, \end{aligned} \tag{B.11}$$

and using lemmas A and B we obtain as a limit

$$I_{m'}^n = \prod_{k=1}^\infty \frac{(n+2k)^2 - m'^2}{(n+2k)^2} e^{im'\pi/2} \int_0^\pi \sin^n \phi \, d\phi. \tag{B.12}$$

According to lemma A the product above is zero if and only if $|m'| = n + 2k$ for $k = 1, 2, 3, \dots$

□

Appendix C. Restricted geometry of $\mathcal{P}(\omega, \mathcal{D})$

By fixing $\varphi = \varphi_0$, multiplying both sides of (46) by $P_l^{m'}(-\hat{\mathcal{D}}) e^{-im'\theta}$ and integrating over $\hat{\mathcal{D}}$ and θ we obtain

$$\begin{aligned} \int_{-1}^1 \int_0^{2\pi} L(\hat{\mathcal{D}}, \theta, \varphi) (1 - \hat{\mathcal{D}}^2)^{-\frac{n}{2}} P_l^{m'}(-\hat{\mathcal{D}}) e^{-im'\theta} \, d\theta \, d\hat{\mathcal{D}} \\ = \frac{4\pi}{2l+1} \frac{(l+m')!}{(l-m')!} e^{im'\pi/2} I_{m'}^n \sum_{m=-l}^l e^{im(\varphi_0+\pi/2)} d_{m'm}^{(l)}(\pi/2) \varrho_{lm}. \end{aligned} \tag{C.1}$$

For a fixed l we have $2l + 1$ equations (one per each m' , $-l \leq m' \leq l$) and unknowns q_{lm} . Let us define a $(2l + 1) \times (2l + 1)$ -matrix

$$\mathbf{M}^{(l)}(\varphi_0) = (M_{m'm})_{\substack{-l \leq m' \leq l \\ -l \leq m \leq l}}, \quad M_{m'm} = e^{im(\varphi_0 + \pi/2)} d_{m'm}^{(l)}(\pi/2), \quad -l \leq m, m' \leq l. \quad (\text{C.2})$$

Since $d_{m'm}^{(l)}(\pi/2) = D_{m'm}^{(l)}(0, \pi/2, 0)$, we have

$$\det \mathbf{M}^{(l)}(\varphi_0) = \exp \left[i(\varphi_0 + \pi/2) \sum_{m=-l}^l m \right] \det D^{(l)}(0, \pi/2, 0) = \det D^{(l)}(0, \pi/2, 0) \neq 0, \quad (\text{C.3})$$

as the rotation matrix $D^{(l)}$ is, of course, invertible. We also define for those m' for which $I_{m'}^n \neq 0$,

$$\mathcal{L}_{m'} = \frac{(2l+1)(l-m')!}{4\pi e^{im'\pi/2} (l+m')! I_{m'}^n} \int_{-1}^1 \int_0^{2\pi} L(\hat{D}, \theta, \varphi_0) (1 - \hat{D}^2)^{-\frac{n}{2}} P_l^{m'}(-\hat{D}) e^{-im'\theta} d\theta d\hat{D}, \quad (\text{C.4})$$

together with

$$\mathcal{L}^{(l)}(\varphi_0) = (\mathcal{L}_{m'})^T = (\mathcal{L}_{-l}, \dots, \mathcal{L}_l)^T \quad \text{and} \quad \varrho^{(l)} = (\varrho_{lm})^T = (\varrho_{l,-l}, \dots, \varrho_{ll})^T. \quad (\text{C.5})$$

Thus we obtain

$$\mathcal{L}^{(l)}(\varphi_0) = \mathbf{M}^{(l)}(\varphi_0) \varrho^{(l)} \quad \text{and} \quad \varrho^{(l)} = [\mathbf{M}^{(l)}(\varphi_0)]^{-1} \mathcal{L}^{(l)}(\varphi_0). \quad (\text{C.6})$$

According to the lemma, (C.6) is valid for every l if n is not an integer ($n > -1$). As n approaches an integer value, $I_{m'}^n$ approaches 0 when $m' + n$ is an even integer and $|m'| > n$. Thus solutions for (C.6) become less and less well determined when $l > n + 1$. Finally, if n is an integer, (C.6) holds true only for $l \leq n + 1$. In this case one phase φ_0 is not sufficient for determining ρ . We have thus proved that if $S = \mu^n$, $n > -1$, and $n \in \mathbb{R}$ is not an integer, two-dimensional $L(\theta, \mathcal{D})$ -data corresponding to any fixed phase φ_0 determine the reflectivity function ρ uniquely. \square

References

- [1] Arfken G 1970 *Mathematical Methods for Physicists* (New York: Academic)
- [2] Ďurech J and Kaasalainen M 2003 Photometric signatures of highly nonconvex and binary asteroids *Astron. Astrophys.* **404** 709–14
- [3] Gardner R J 1995 *Geometric Tomography* (Cambridge: Cambridge University Press)
- [4] Gardner R J and Milanfar P 2003 Reconstruction of convex bodies from brightness functions *Discrete Comput. Geom.* **29** 279–303
- [5] Hestroffer D, Tanga P, Cellino A, Guglielmetti F, Lattanzi M, DiMartino M, Zappala V and Berthier J 2002 Asteroid observations with the Hubble Space Telescope FGS *Astron. Astrophys.* **391** 1123–32
- [6] Hudson R S and Ostro S J 1990 Doppler radar imaging of spherical planetary surfaces *J. Geophys. Res.* **95** 10.947–63
- [7] Kaasalainen M 1990 On the inverse problem of asteroid lightcurves *MSc Thesis* University of Helsinki
- [8] Kaasalainen M, Lamberg L, Lumme K and Bowell E 1992 Interpretation of lightcurves of atmosphereless bodies. I. General theory and new inversion schemes *Astron. Astrophys.* **259** 318–34
- [9] Kaasalainen M and Torppa J 2001 Optimization methods for asteroid lightcurve inversion. I. Shape determination *Icarus* **153** 24–36
- [10] Kaasalainen M, Torppa J and Muinonen K 2001 Optimization methods for asteroid lightcurve inversion. II. The complete inverse problem *Icarus* **153** 37–51
- [11] Kaasalainen M 2001 Interpretation of lightcurves of precessing asteroids *Astron. Astrophys.* **376** 302–9

- [12] Kaasalainen M 2004 Physical models of large number of asteroids from calibrated photometry sparse in time *Astron. Astrophys.* **422** L39–42
- [13] Kaasalainen M, Hestroffer D and Tanga P 2005 Physical models and refined orbits for asteroids from Gaia photo- and astrometry *The Three-dimensional Universe with Gaia* (ESA SP-576) pp 301–4
- [14] Kaasalainen S, Kaasalainen M and Piironen J 2005 Ground reference for space remote sensing: laboratory photometry of an asteroid model *Astron. Astrophys.* **440** 1177–82
- [15] Kaipio J and Somersalo E 2005 *Statistical and Computational Inverse Problems* (New York: Springer)
- [16] Lamberg L 1993 On the Minkowski problem and lightcurve operator *PhD Thesis* University of Helsinki
- [17] Lamberg L and Kaasalainen M 2001 Numerical solution of the Minkowski problem *J. Comp. Appl. Math.* **137** 213–27
- [18] Lehtinen M, Markkanen J, Väänänen A, Huuskonen A, Dantie B, Nygren T and Rahkola J 2002 A new incoherent scatter technique in the EISCAT Svalbard radar *Radio Sci.* **37** 101.1029–1043
- [19] Marchis F, Kaasalainen M, Hom E, Berthier J, Enriquez J, Hestroffer D, Le Mignant D and de Pater I 2006 Shape, size and multiplicity of main-belt asteroids. I. Keck adaptive optics survey *Icarus* at press
- [20] Minkowski H 1903 Volumen und Oberfläche *Math. Ann.* **57** 447–95
- [21] Nathues A, Mottola S, Kaasalainen M and Neukum G 2005 Spectral study of the Eunomia asteroid family. I. Eunomia *Icarus* **175** 452–63
- [22] Nirenberg L 1953 The Weyl and Minkowski problems in differential geometry in the large *Commun. Pure Appl. Math.* **6** 337–94
- [23] Ostro S J and Connelly R 1984 Convex profiles from asteroid lightcurves *Icarus* **57** 443–63
- [24] Ostro S J, Hudson R S, Benner L, Giorgini J, Magri C, Margot J-L and Nolan M 2002 Asteroid radar astronomy *Asteroids III* (Tucson, AZ: Arizona University Press)
- [25] Press W, Flannery B, Teukolsky S and Vetterling W 1990 *Numerical Recipes* (Cambridge: Cambridge University Press)
- [26] Russell H N 1906 On the light-variations of asteroids and satellites *Astrophys. J.* **24** 1–18
- [27] Wahba G 1990 *Spline Models for Observational Data* (Philadelphia, PA: Society for Industrial and Applied Mathematics)
- [28] Weissbluth M 1980 *Atoms and Molecules* (New York: Academic)